**ORIGINAL PAPER**

# Carbon-based nanohybrid fabricated in-situ and boosted the adsorption of anionic reactive yellow dye

N. A. Fathy[1] 🔵 · S. El-Shafey[1]

## Abstract

The purpose of this research is to report a unique manipulation of producing carbon nanotubes/carbon xerogel (CNTs/CX) hybrid loaded with bimetallic catalysts of Fe–Ni via one-step chemical vapor deposition (CVD) of camphor. Active bimetallic catalysts were formed during carbonization of resorcinol–formaldehyde xerogel at 800 °C to form carbon xerogel (CX); meanwhile, the carbon gas was librated from camphor at 220 °C for 45 min. CX and CNTs/CX samples were analyzed using measurements of transmission electron microscope (TEM), X-ray diffraction tool (XRD) and Fourier transform infrared spectroscopy (FTIR). Further, the liquid-phase adsorption of a reactive yellow 160 (RY160) dye on CX and CNTs/CX samples and thermodynamic studies were investigated. TEM and XRD results revealed the formation of carbon nodules in CX combined with bundles of CNTs having outer diameters ranged from 40 to 80 nm in CNTs/CX. Adsorption of RY160 dye was highly relied on pH, temperature, initial dye concentration and contact time. Through kinetic modeling, pseudo-second-order kinetic model expressed closely the experimental data of RY160 adsorption. Equilibrium adsorption studies declared that the Freundlich model is the better with adsorption of RY160 on CNTs/CX due to it has heterogeneous surface character resulting from combination of CX and CNTs. Langmuir adsorption capacity ($q_L$, mg/g) values exhibited that CNTs/CX sample have a superior adsorption of RY160 dye which were reached to 167 mg/g than that by CX ($q_L = 125$ mg/g). Thereof, the produced CX and CNTs/CX samples present higher removal capacity and can be employed successfully for RY160 dye removal from a textile wastewater.

**Keywords** Carbon nanotubes/Carbon xerogels nanohybrid · Liquid-phase adsorption · Reactive yellow dye · Wastewater treatment

## Introduction

This modern era endorses rapid developments in the synthesis of carbon materials in nanometric forms to use them in the advanced technological and industrial fields (Fathy 2020; Fathy et al. 2019a; Laurila et al. 2017). For example, carbon-based nanostructures (e.g., carbon nanotubes, graphene, carbon nanofibers, etc.) have attracted a significant attention in manufacturing electronic devices, heat insulators, plane/automotive parts and in biomedical, clean/storage energy

and purification applications (Navrotskaya et al. 2020; Fathy et al. 2017a, b; Annamalai et al. 2017; Chinnappan et al. 2016; Li et al. 2014; Halama et al. 2010). These materials consist mainly of carbon atoms formed at nanoscale, for example; carbon gels, carbon nanofibers, carbon nanotubes, graphenes, nanodiamonds, fullerenes and carbon dots which have unique electronic, optical, thermal, mechanical, and chemical properties. For instance, carbon xerogels (CXs) as a part of carbon gels are produced from polycondensation of resorcinol and formaldehyde in acidic or basic medium followed by drying in a conventional oven then carbonization in an inert gas medium at elevated temperature (Arenillas et al. 2019; Rashwan et al. 2018; Celzard et al. 2012; Zubizarreta et al. 2008; Job et al. 2005). CXs have concerned a considerable attention due to their controllable and tunable porosity, thus can be manufactured in suitable forms; e.g., monoliths, thin films and pellets on a large-scale for a

✉ N. A. Fathy
fathyna.77@hotmail.com

[1] Physical Chemistry Department, National Research Centre, 33 El Bohouth Street (former Tahrir st.), Dokki, P.O. 12622, Giza, Egypt

specific applications (Kicínski et al. 2021; Arenillas et al. 2019; Zubizarreta et al. 2008; Job et al. 2005).

Regarding to its tubular shapes and high aspect ratio, carbon nanotubes (CNTs), which had been discovered by Iijima (1991); possess excellent chemical and physical properties that related to robustness (Young's Modulus[3]1 Tpa), chemical inertness, electrical and thermal conductivity (De Volder et al. 2013; Mukul et al. 2002). Current methods applied in synthesis of CNTs are; arc-discharge, laser ablation and chemical vapor deposition (CVD) from catalytic decomposition of hydrocarbons on transition metals (Huang et al. 2012; Prasek et al. 2011; Zhang et al. 2011).

In recent years, carbon nanostructures can be formed hybrids or composites with other inorganic or organic materials in order not only to combine the properties of individual components but also to create synergistic effects for boosting their final properties (El-Khouly et al. 2020; Fathy et al. 2019b; Shouman and Fathy 2018). For instance, nanocarbon hybrids were fabricated from carbon xerogels with carbon nanotubes were used as efficient adsorbents in the removal of dyes (Fathy et al. 2019b; Shouman and Fathy 2018), heavy metals (Embaby et al. 2021) and as supercapacitors (Fathy et al. 2017a, b). It has been found that the surface area of CNTs/CX > CX when CNTs powder was embedded directly through sol-gel of resorcinol–formaldehyde precursors and then exposed to carbonization (Shouman and Fathy 2018; Haghgoo et al. 2015), but it decreased when CNTs synthesized over CX through carbonization of resorcinol–formaldehyde xerogels (Fathy et al. 2017a, b). However, the produced CNTs/CX hybrids through carbonization of organic xerogel gave superb adsorption capacity, photocatalytic activity and high supercapacitance (Fathy et al. 2019b; 2017a, b). In previous studies, authors have implemented the combination of CNTs with carbon aerogels through sol-gel process (Worsley et al. 2009; Haghgoo et al. 2014). Lately, Fathy and coworkers interested in fabrication of carbon nanotubes and other carbon nanostructures by solid-state transformation over carbon xerogels as substrate during CVD of camphor as CNTs source. They applied different types of catalysts such as Ni catalyst (Fathy et al. 2017a), Ni–Fe di-catalysts (Fathy et al. 2019b) and Fe–Ni–Cu tri-catalysts (Fathy et al. 2017b), which have been inserted by wet impregnation onto the surface of organic xerogels. It has been observed that the final morphology and yield of CNTs over CX are correlated basically with the catalyst type and size.

The presence of considerable amounts of dyes is considered to be a serious concern. Because of its toxicity and non-degradability, dye pollution poses a rigorous hazard to the environment and human health. Particularly, reactive dyes are the most common dyes which used extensively in large amounts through the dyeing process in textile, leather, pulp and paper, plastics, tanneries, and food companies due to its bright color, good color fastness, and ease of applications (Bedolla-Guzman etal. 2016). The adsorption using porous carbon materials is the best technique to reuse the dye-contaminated water, as compared to chemical, physical and biological processes, owing to it is easy procedure and can effectively remove various contaminants from the aquatic environment without any secondary pollution (Girgis et al. 2011). The current work explains the morphology and adsorption characteristics of CNTs obtained over CX substrate in the presence of bimetallic catalysts of iron and nickel loaded onto organic xerogel during the co-precipitation process. Beside this, the adsorption properties of yielded carbon-based nanohybrid with comparing to parent CX sample were investigated through removal studies of anionic reactive dye from their aqueous media under different conditions.

Therefore, we report here a new approach for decoration of carbon xerogels with carbon nanotubes (CNTs) through in situ chemical vapor deposition (CVD) of camphor as a carbon gas precursor. Morphology, surface, and adsorptive characteristics of carbon xerogel (CX) before and after decoration with as-prepared carbon nanotubes were investigated. Fe and Ni salts were loaded onto resorcinol–formaldehyde organic xerogel by co-precipitation route and then chemically reduced to bimetallic catalysts during carbonization of organic xerogel and CVD of camphor simultaneously. Textile azo dye such as a reactive yellow 160 dye was used to study the adsorption performance of CX and CNTs/CX nanohybrid under different adsorption conditions.

## Materials and methods

### Materials

Resorcinol ($C_6H_6O$, Panreac, 99%), formaldehyde (HCHO, Adwic, 36–38%), methanol ($CH_3OH$, Sigma-Aldrich, 99%), sodium carbonate ($Na_2CO_3$, POCH SA, 99%), Sodium hydroxide (NaOH, Panreac, 98%), ferric nitrate (Fe$(NO_3)_3 \cdot 9H_2O$, Sigma-Aldrich, 98%) and nickel nitrate (Ni$(NO_3)_2 \cdot 6H_2O$, Sigma-Aldrich, 99.8%), and laboratory distilled water were used.

### Preparation of Resorcinol–formaldehyde (RF) xerogel supported catalysts

The RF xerogel was prepared through sol-gel of resorcinol with formaldehyde (1:2 molar) in presence of $Na_2CO_3$ as basic catalyst, adapting the procedure described elsewhere (Fathy et al. 2017a and 2019b). After drying at 100 °C overnight, the obtained xerogel was ground to be used as a support for Fe and Ni catalysts. Preparation of the bimetallic catalysts supported on resorcinol formaldehyde xerogel

by a co-precipitation method was performed in mass percent of RF: Fe–Ni = 80:20. A mixture solution containing iron nitrate (Fe(NO₃)₃·9H₂O) and nickel nitrate (Ni(NO₃)₂·6H₂O) was added to desired amount of RF xerogel powder in a beaker under stirring with heating at 50 °C followed by adding 0.5 M NaOH drop by drop to adjust pH at 9 at which hydroxides of Fe and Ni will be precipitated. Co-precipitation of hydroxides over RF xerogel sample is left under stirring and heating for 60 min, and then hold overnight at room temperature. After that, the product was washed with distilled water and ethanol throughout filtration and dried at 80 °C overnight.

## Growth procedure of CNTs over carbonized RF xerogel

Synthesis of CNTs using CVD over carbonized RF xerogel supported with Fe and Ni was followed the procedure prescribed previously (Fathy et al. 2017a) using a stainless steel tube (diameter = 32 mm and length = 80 mm) which was placed horizontally along two electric furnaces. The camphor was put in an alumina boat and kept inside the first furnace. In the 2nd furnace, RF xerogel supported with Fe and Ni was put in an alumina boat and heated at 800 °C under passing nitrogen gas. When camphor was heated at 220 °C to get the carbon in a gas phase, the temperature of 2nd furnace was set at 800 °C for growing CNTs on the surface of pyrolyzed RF xerogel, where the insert N₂ gas is a carrier for carbon vapors liberated from camphor to transfer to the 2nd furnace. The growth time for CNTs production was set up to 45 min and then the two furnaces were switched off. The resulting black product formed inside the 2nd furnace tube in the high temperature zone was collected and labeled as CNTs/CX hybrid.

## Characterization of carbon samples

The prepared samples were characterized with reference to their morphologies before and after formation of CNTs. High-resolution transmission electron microscopy (HR-TEM, JEM-1230, Japan) was used to determine the morphology of the resulting carbon samples. The crystalline phases in the obtained samples were determined by X-ray diffraction analysis using a Bruker diffractometer (Bruker D8 advance, Germany). The patterns were run with CuKα1 target with secondly monochromator 40 kV, 40 mA. The characteristic surface functional groups developed on the surface of CNTs were investigated by Fourier transform infrared (FTIR) spectroscopy in the range of 4000–400 cm⁻¹ using KBr disc technique (JASCO 6100 FTIR spectrometer, Japan).

## Adsorption studies

Batch adsorption experiments were carried out toward a reactive yellow 160 (RY160) dye to demonstrate the adsorption capacity of the carbon samples. About 20 mL of RY160 dye solutions with different initial concentrations of 25 to 500 mg/L were conducted with 20 mg of adsorbent under shaking at 200 rpm and 25 °C for 24 h. The pH effect on the dye adsorption efficiency was investigated using an initial pH range of 2–8 with 20 mg of adsorbent and 50 mg/L of initial dye concentration for 2 h. Influence of temperature (25, 40 and 55 °C) with 50 mg/L of initial dye concentration was studied at working pH of dye of 4.0, fixed mass of carbon of 20 mg, and magnetic stirring of 200 rpm, respectively. Moreover, kinetic adsorption studies were performed for 50 mg of adsorbent with 50 and 100 mg/L of dye solution (50 mL) at 25 °C, under magnetic stirrer at 200 rpm, within contact time ranging from 5 to 120 min. The dye concentrations in the filtrate were determined using a UV–visible spectrophotometer (Shimadzu Model PC-2401) by measuring the maximum absorbance at a wavelength of 425 nm. Duplicate absorbance readings were recorded for each experiment. All absorbance results were calculated by taking the mean of two readings of absorbance and found that their relative errors were below 5%.

The amount of adsorbed dye was calculated from the mass balance expression given by:

$$q_e = \frac{(C_o - C_e)}{m} V \tag{1}$$

where $q_e$ is the amount of adsorbed dye by the adsorbents (mg/g), $C_o$ is initial ion concentration of RY160 dye (mg/L), $C_e$ is equilibrium concentration of RY160 dye (mg/L), $m$ is the mass of adsorbent in (mg) and $V$ is the volume of RY160 solution in contact with the adsorbent (mL). Langmuir, Freundlich and Tempkin models were used to analyze the adsorption of RY160 dye onto the investigated samples. In addition, the data of kinetic adsorption were analyzed in terms of three kinetic models such as pseudo-first-order Lagergren, pseudo-second-order and intraparticle diffusion.

## Results and discussion

### Morphology investigation of prepared samples

The morphology of the prepared carbon xerogel (CX) before and after loading of bimetallic catalyst of Fe–Ni metals by coprecipitation followed by carbonization of RF gels at 800 °C for 45 min under flowing of N₂ gas was investigated using TEM as shown in Fig. 1A and B. It can be seen that the surface of carbon xerogel shows formation of interconnected

**Fig. 1** TEM micrographs of carbon xerogels **A** CX and **B** Fe–Ni/CX prepared at 800 °C for 45 min (black shadow in Fig. 2 refers to catalysts)
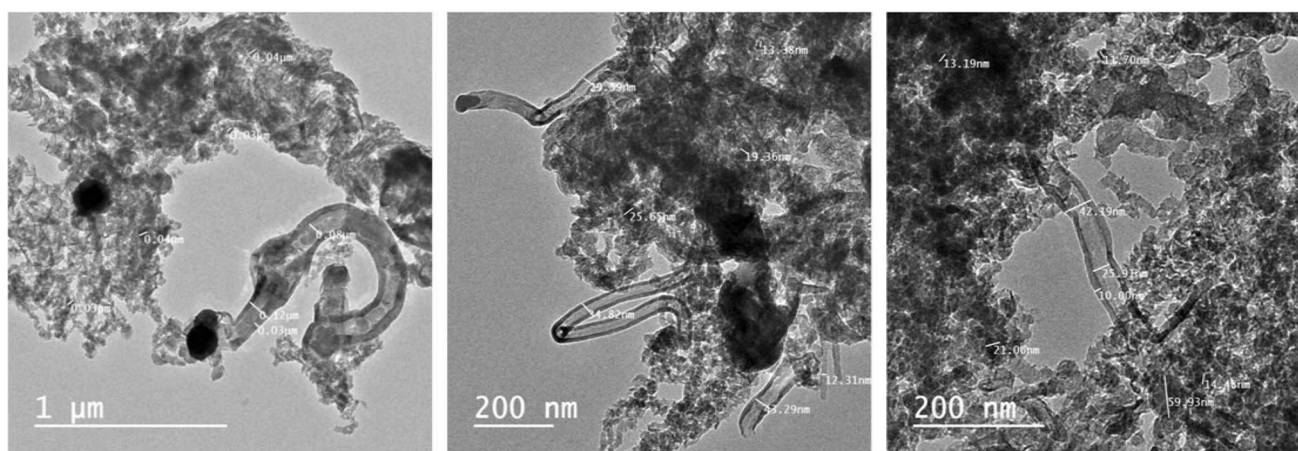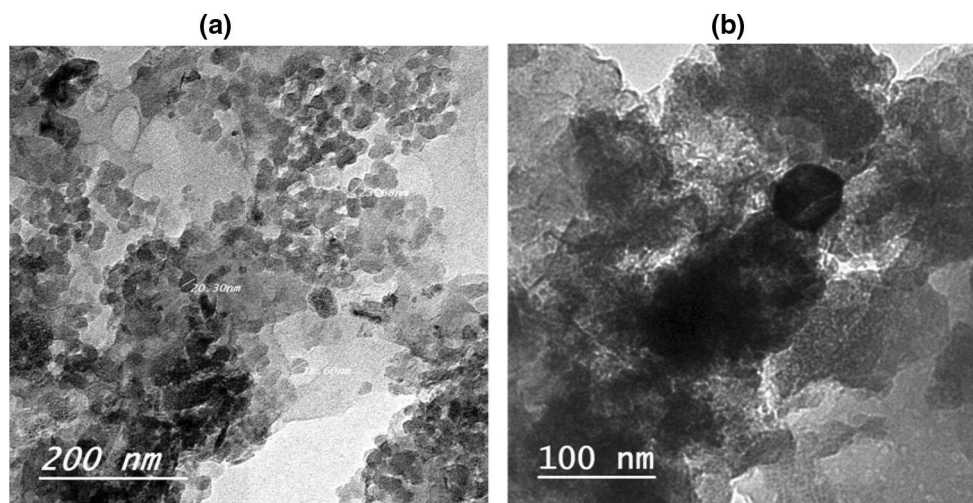
**(a)**    **(b)**





**Fig. 2** TEM images of CNTs/CX sample prepared from CVD of carbon gas produced from cracking of camphor at 220 °C on pyrolyzed surface of Fe–Ni/CX at 800 °C for 45 min

spherical nodules with average sizes ranged from 20 to 40 nm without loading of a bimetallic catalyst. The presence of catalysts at carbonization temperature of 800 °C led to an intrinsic change in the surface of CX. It could be enhanced the surface graphitization of carbon xerogels and decreased both the interparticle distances and particle sizes of nodules to less than 20 nm which is promoting the surface performance of CX to build CNTs as seen in Fig. 2.

Figure 2 describes the TEM images for the surface of CNTs/CX sample prepared from CVD of carbon gas produced from cracking of camphor at 220 °C on pyrolyzed surface of Fe–Ni/CX at 800 °C for 45 min. The obtained CNTs through the prescribed system have different structures and outer diameters ranged from 40 to 80 nm along the CX matrix. Yield of produced CNTs/CX was reached to about 25% as compared with our previous studies. This may be attributed to the nano-sizes of Fe–Ni bimetallic catalyst formed over the surface of CX. Therefore, it can be

concluded that the surface of Fe–Ni/CX loaded by co-precipitation is an effective substrate to establish well-bundles of CNTs.

Figure 3 compares the XRD patterns of both prepared samples, i.e., CX (loaded Fe–Ni) and CNTs/CX (loaded Fe–Ni). XRD patterns for CX sample showed a broad peak at $2\theta = 25°$ with corresponding $d$-spacing value of 3.56 Å, indicating the presence of amorphous carbon xerogel. Upon deposition of CNTs on CX surface, the intensity and phases in XRD patterns of CX are changed obviously. Width of peak at $2\theta = 25°$ is decreased to half with appearing two crystalline peaks at $2\theta = 43.5°$ and 50.8°, which are assigned to: (i) Formation of CNTs combined with CX matrix and (ii) Creation of Fe and Ni binary metals (PDF#00-018-0877) on CX obtained during CVD of camphor with corresponding d-spacing values of 2.07 and 1.78 Å (Fang et al., 2020), respectively. This result confirms the formation of Fe–Ni bimetallic catalysts on CX as resulting from a reduction
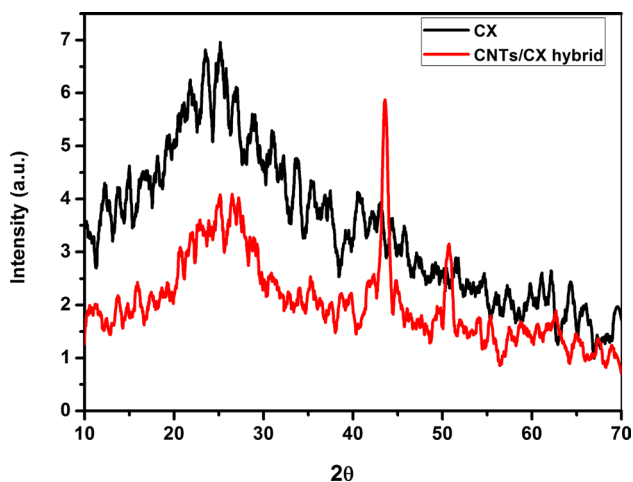
**Fig. 3** XRD profiles of CX and CNTs/CX samples

process happened through flowing carbon gas produced from camphor cracking at 220 °C.

## Surface characteristics of samples by FTIR

Identification of surface characteristics for solid samples is very important to determine their adsorption properties in a liquid-phase adsorption. By measuring the slurry or surface pH of both CX and CNTs/CX samples, it was found that pH values were 4.5 and 4.1, respectively. This observation affirms that the surface of prepared carbons is an acidic in nature where the concentration of acidic groups is somewhat higher than the concentration of basic groups. Moreover, FTIR spectra of the samples and their corresponding results after adsorption of RY 160 dye are investigated as shown in Fig. 4. Before and after adsorption, two FTIR spectra of CX and CNTs/CX samples are significantly different in both position and intensity of their absorption bands as listed in
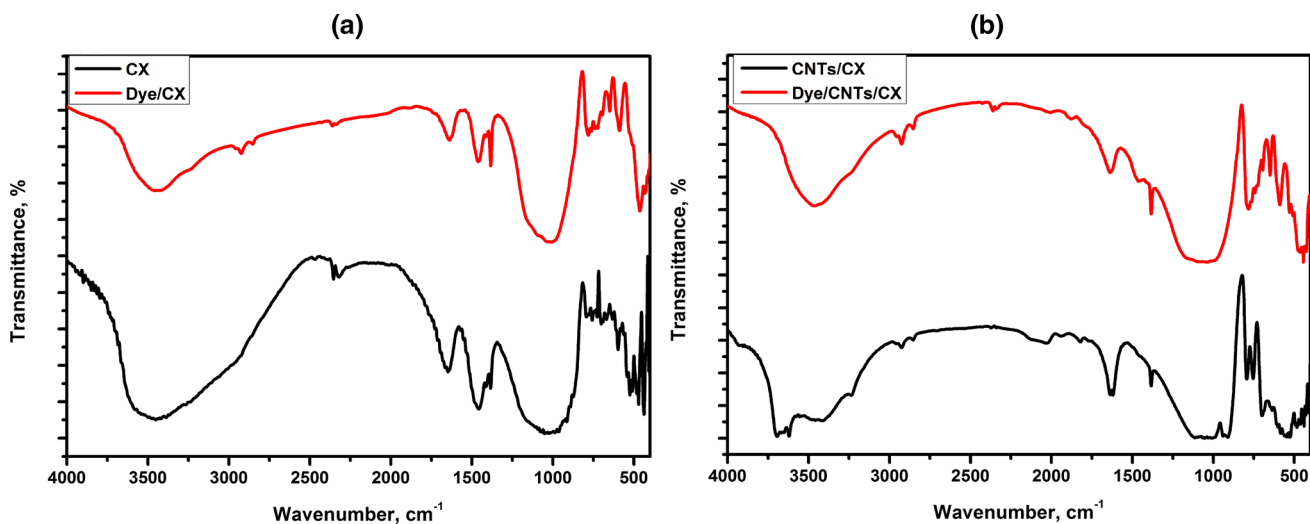


**Fig. 4** FTIR spectra of **A** CX before and after RY160 dye adsorption and **B** CNTs/CX hybrid before and after RY160 dye adsorption

**Table 1** FTIR absorption peak assignments in the prepared samples

| CX | Dye/CX | CNTs/CX | Dye/CNTs/CX | Peak assignments |
|---|---|---|---|---|
| 3470 | 3457 | 3619, 3407 | 3477 | O–H stretching vibration |
| – | 2920, 2848 | 2930, 2846 | 2924, 2852 | C–H stretching vibration (asymmetric and symmetric) |
| 2355, 2318 | 2366, 2330 | 2368, 2325 | 2369 | C=C conjugated |
| 1643 | 1637 | 1631 | 1636 | $\nu$(C=C) and $\nu$(C=O) of inter-ring chain |
| 1456 | 1456 | – | – | $CH_3$ bending vibration |
| 1384 | 1379 | 1389 | 1383 | C=O stretching symmetric in $COO^-$ |
| 1017 | 1035 | 1039 | 1062 | C–O–C stretching vibration |
| 780–433 | 776–462 | 790–482 | 785–452 | C–H, C–M |

Table 1. Where, Table 1 indicates the peak assignments of functional groups formed on the prepared samples. Results confirm that the formation of CNTs over CX produced through carbonization of resorcinol–formaldehyde xerogel and CVD of camphor changes significantly the surface functional groups of CX. Thus the adsorption of dye molecules has happened through the surface attractions with these oxygen functional groups over both samples. The shoulder absorption bands between 800 and 400 cm$^{-1}$ are related to C–H out-of-plane bending vibrations in the aromatic ring which bonded with bimetallics formed over CX (Atieh et al., 2010). Moreover, the reduction in the intensity of adsorption bands related to OH, COOH and C–O–C groups is observed, confirming the surface attractions of these groups with the adsorbed dye molecules.

## Adsorption studies

### Effect of pH

The influence of pH on the adsorption ability of carbon adsorbents toward anionic RY160 dye was determined by varying pH values from 2 to 8 at fixed initial dye concentration of 50 mg/L, 20 mg of carbon dose and 25 °C. The results of removal efficiency of dye using samples as a function of pH are depicted in Fig. 5. Adsorption process showed a noticeable effect of pH, with increasing pH value the adsorption of RY160 is decreased. Thus, the highest adsorption occurred at pH 2, while the lowest happened at pH 8. At acidic medium, the sulphonate groups ($SO_3^-$) of RY160 dye of negatively charged and the hydroxyl groups of the adsorbent that are protonated by H$^+$ ions of positively charged forming a strong electrostatic attraction between oppositely char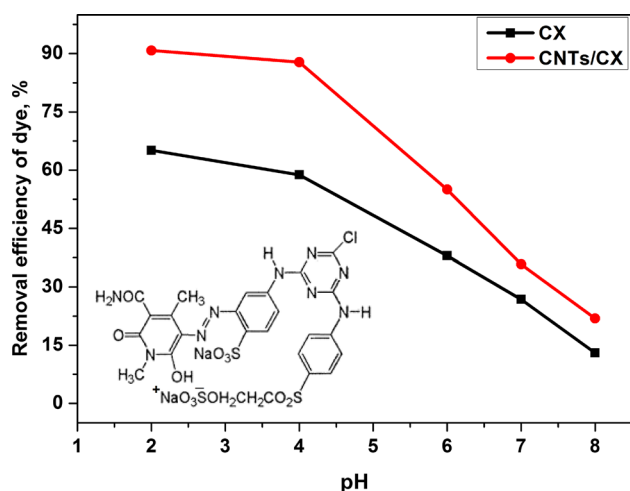ges, accordingly the adsorption process increases. Inversely, with increasing pH value, the repulsion forces are obtained between OH$^-$ of the adsorbent and $SO_3^-$ groups of dye as well as the competition between the negatively charged groups of dye and OH$^-$ of basic medium. These results agree with the previous data in the literature (Toutounchi et al. 2019; Abdel Ghafar et al. 2020a, b; Kiran et al. 2020; Shariati et al. 2021). In the next experiments, we carried out the adsorption of dye at the working pH of dye (pH = 4) without adjusting.

### Effect of temperature and thermodynamic studies

Figure 6A presents the relation between the removal efficiency of dye over carbon adsorbents and the change in temperature. Results obtained showed a perceptible decrease in the removal efficiency of RY160 dye from 59 and 85% to 22 and 45% onto CX and CNTs/CX, respectively; with an increase in temperature from 25 to 55 °C. This affirms that the adsorption process of RY 160 is exothermic in nature. Thus adsorption of RY160 dye at a lower temperature is a favorable. Also, the negative values of enthalpy energy (ΔH°) confirm this nature (Barka et al. 2011; Younes et al. 2021).

Thermodynamic activation parameters involving ΔH° (enthalpy), ΔS° (entropy) and ΔG° (Gibbs free energy) were calculated to state the thermodynamic nature of the adsorption process of RY160 dye, ΔG° was determined using Van't Hoff equation equation (Kousha et al. 2015);

$$\ln K_d = -(\Delta G^\circ / RT) \tag{2}$$

where ($K_d = q_e/C_e$) represents the distribution coefficient constant, $R$ is the general gas constant (8.314 J/mol Kelvin) and T is the absolute temperature (Kelvin). Since ΔG° can be also given as follow:

$$\Delta G^\circ = \Delta H^\circ - T\Delta S^\circ \tag{3}$$

From Eqs. 2 and 3:

$$\ln K_d = (\Delta S^\circ / R) - (\Delta H^\circ / RT) \tag{4}$$

A linear relation was obtained from plotting of $\ln K_d$ with 1/T (Fig. 6B), from the slope and intercept of this plotting, ΔH° and ΔS° parameters were calculated, respectively, and listed with the other parameters in Table 2. From this table, negative value of ΔH° appearing the exothermic nature of the adsorption process. Values of ΔS° are negative that imply decreasing the randomness at the solid/ solution interface. The negative values of ΔG° showed that the adsorption process is feasible and spontaneous. In addition, there is a decrease in the ΔG° values with increasing temperature suggesting that the RY160 dye uptake is a great favourite. Also, the values of ΔG° are less than −40 kJ/mol, meaning that the interaction between dye molecules and adsorbent surface
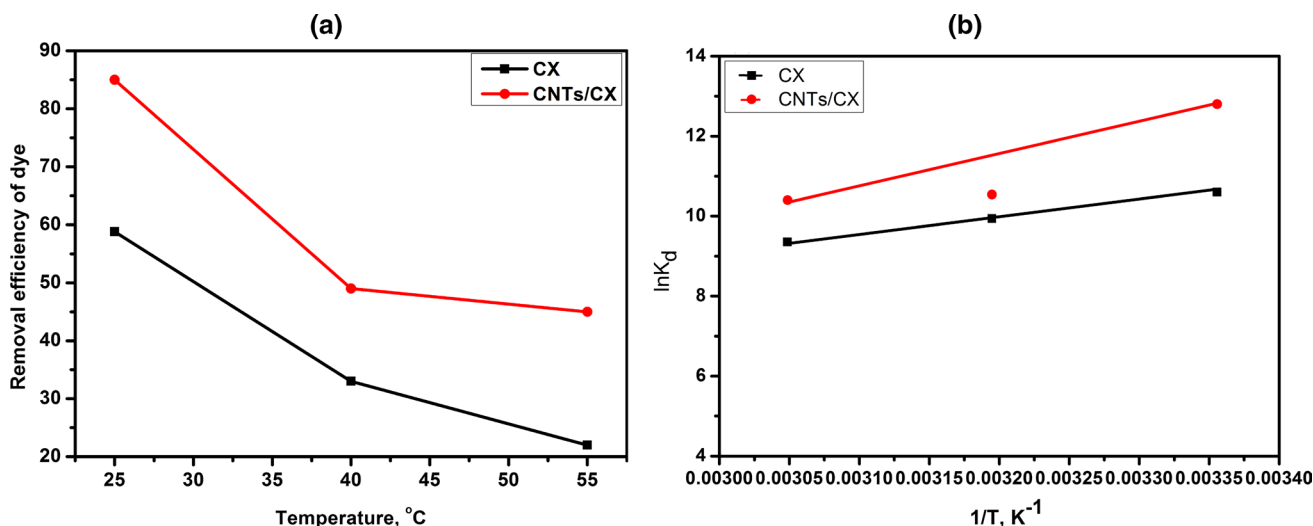


**Fig. 5** Effect of pH on the adsorption of RY160 onto carbon adsorbents ($C_0$ = 50 mg/L, dose = 20 mg, $T$ = 25 °C, and contact time = 2 h)

**Fig. 6 A** Effect of temperature on removal efficiency of RY160 dye and **B** plot of $\ln K_d$ against 1/T ($C_0 = 50$ mg/L, dose $= 20$ mg, and contact time $= 2$ h)

**Table 2** Thermodynamic parameters for the uptake of RY160 by samples

| Adsorbents | Temp. (K) | $\Delta G°$ (kJ/mol) | $\Delta H°$ (kJ/mol) | $\Delta S°$ (J/mol K) |
|---|---|---|---|---|
| CX | 298 | −26.32 | −33.53 | −24.19 |
| | 313 | −25.95 | | |
| | 328 | −25.59 | | |
| CNTs/CX | 298 | −30.98 | −64.97 | −114.1 |
| | 313 | −29.27 | | |
| | 328 | −27.56 | | |

may be controlled by a physisorption mechanism (Indhu and Muthukumaran, 2018).

### Effect of initial dye concentrations and contact time

In Fig. 7A, the impact of initial dye concentrations on the amount adsorbed of RY160 dye and its removal percentage by studied samples are presented at fixed variables (carbon dose $= 20$ mg, pH $= 4.0$, $V = 20$ ml, contact time $= 24$ h and temperature $= 25$ °C). As it clear, the amount adsorbed of dye is increased gradually with the increase in initial dye concentration ($C_0$, mg/L), on the other hand, the removal percentage (%R) is decreased due to the relationship between %R and $C_0$ is a reversible correlation. The maximum adsorbed amounts of dye onto CX and CNTs/CX were 73 and 112 mg/g with %R of 14.6 and 22.4% at $C_0 = 500$ mg/L, respectively. At $C_0 = 25$ mg/L, the maximum

removal of RY150 dye onto CX and CNTs/CX samples values were 31.1 and 50.4%, respectively.

Results regarding to effect of contact time as initial dye concentration changed with time on the adsorbed amount of dye ($q_t$, mg/g) is given in Fig. 7B. With an increase in contact time from 5 to 180 min, the adsorbed amount of dye is increased substantially (5–24 mg RY160/g CX and 16–38 mg RY160/g CNTs/CX) over both samples at an initial dye concentration of 50 mg/L. With increasing an initial dye concentration from 50 to 100 mg/L, CNTs/CX exhibited higher amount adsorbed of RY160 dye (27–50 mgRY160/g CNTs/CX) as shown in Fig. 7B. Furthermore, these results revealed that the uptake rates of RY160 dye on CNTs/CX were fast in the first 5 min and gradually decreased with time till equilibrium. This is attributed to the availability of a large number of active sites on the surface of sample, and then the adsorption rate decreases with the gradual occupancy of these sites (Kiran et al. 2020; Shariati et al. 2021; Younes et al. 2021). Moreover, the equilibrium time can be attained within 60 min over CX and CNTs/CX surfaces.

### Kinetic studies

In order to determine the kinetic order and adsorption behavior of the studied dye on sample prepared in this study, Fig. 8A–C is analyzed using pseudo-first-order, pseudo-second-order and intra-particle diffusion models. Table 3 summarizes the calculated values of the maximum amount adsorbed, rate constants and the correlation coefficients ($R^2$) of the applied kinetic models (Lagergren 1898; Ho and McKay, 1998; Morris and Weber, 1963). The correlation coefficients of the second-order model ($R^2 > 0.98$) were

**Fig. 7** Effect of **A** initial dye concentrations and **B** contact time on the removal of RY160 dye by studied samples (carbon dose = 20 mg, pH = 4.0, V = 20 ml, contact time = 24 h and temperature = 25 °C)
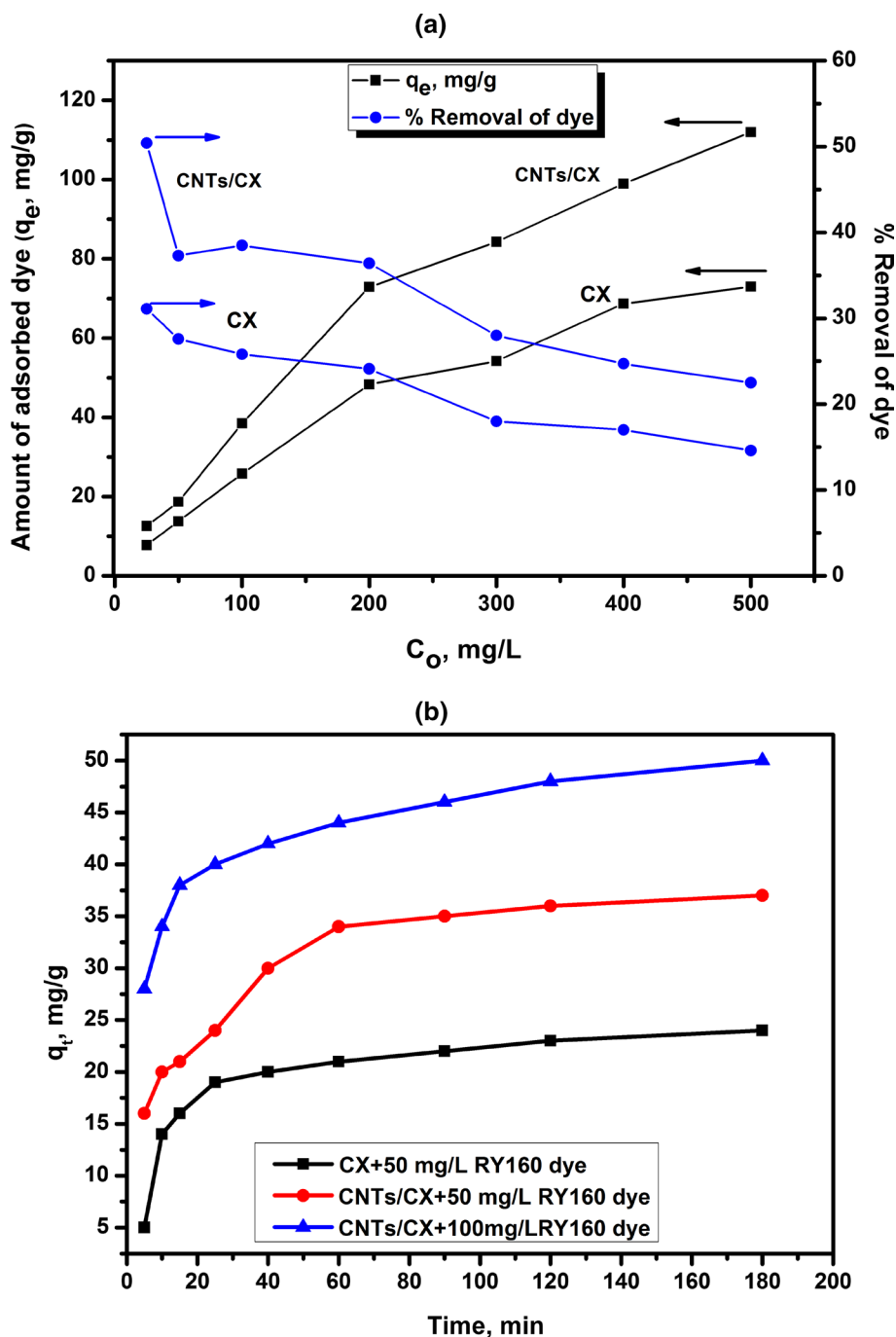


larger than that of the first-order model. Moreover, the calculated value of $q_{e,cal}$ was close to the experimental value ($q_{e,exp}$) for the second-order model. Therefore, the adsorption of RY160 onto both samples obeys a pseudo-second-order model, showing linear plots of pseudo-second-order model (Fig. 8B). This model postulates that the rate-controlling step may be governed by chemisorption sharing or exchange electrons between dye and functional surface groups of carbon (Younes et al. 2021; Indhu and Muthukumaran, 2018; Fathy 2020).

Further in Table 3; $k_1$ is the rate constant of the pseudo-first-order equation (1/min), $q_{e,cal}$ is the calculated adsorption capacity from the model (mg/g). The values of $k_1$ and $q_{e,cal}$ were determined from the slope and intercept of the linear plot of log ($q_e - q_t$) with time. $k_2$ is the constant rate of the pseudo-second-order equation (g/mg min) and calculated from intercept of the linear plot of t/qt against time as shown in Fig. 8. $k_d$ is the rate constant and intercept of intraparticle diffusion equation (mg/g min$^{1/2}$) and $C$ is the intercept of intraparticle diffusion equation, both calculated
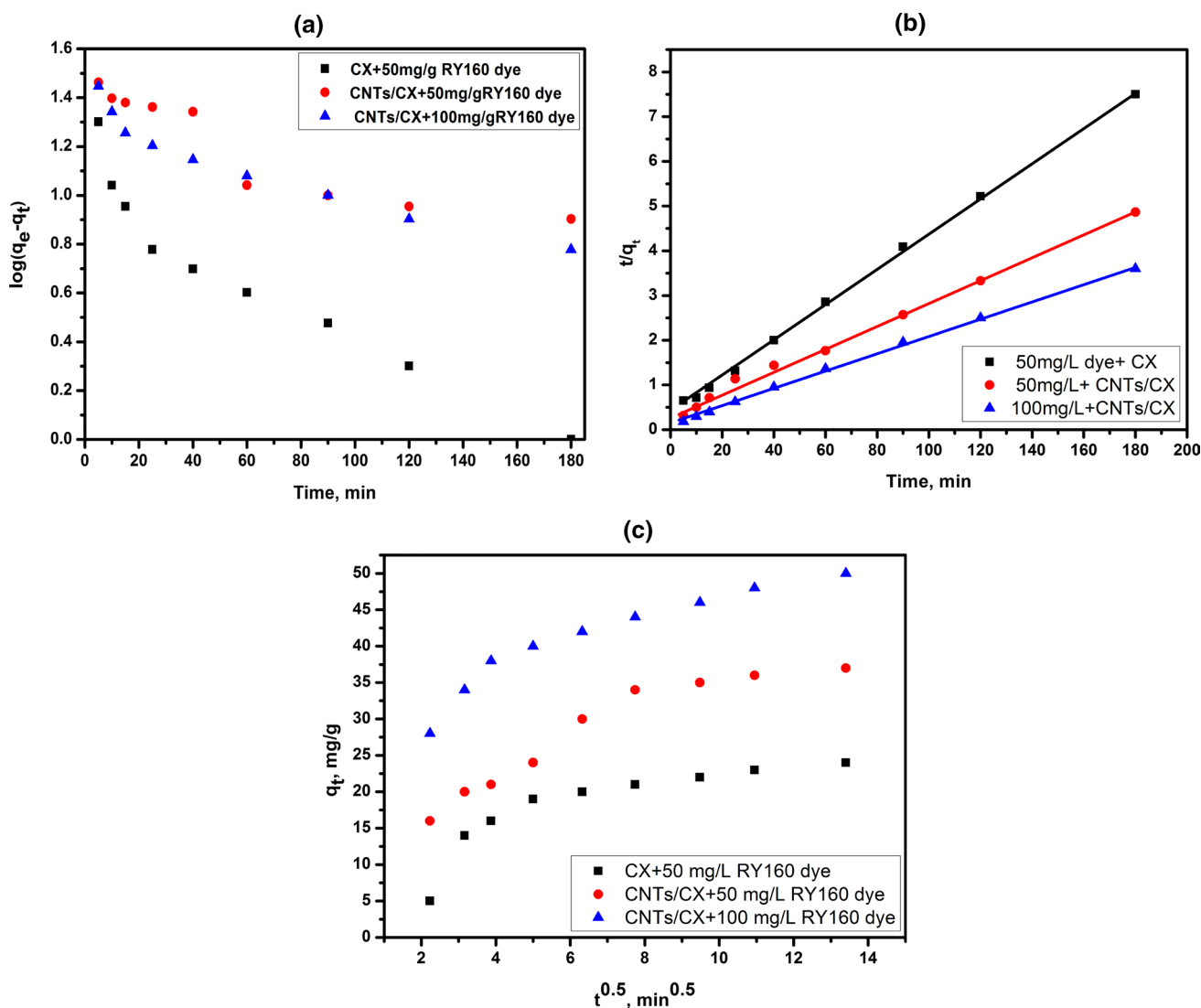
**Fig. 8** **A** Plots of the pseudo-first- order kinetic model, **B** Plots of the pseudo-second-order kinetic model, and **C** Plots of intraparticle diffusion model for the RY160 dye adsorption onto carbon samples (pH = 4, and $T$ = 25 °C)

**Table 3** Adsorption kinetic equation and linear fit parameters for the adsorption of reactive yellow dye onto samples (pH = 4 and $T$ = 25 °C)

| Models | Equation | Parameter | CX | CNTs/CX | |
|---|---|---|---|---|---|
| | | | $C_0 = 50$ mg/L | $C_0 = 50$ mg/L | $C_0 = 100$ mg/L |
| Pseudo-first-order | $\log\left(q_e - q_t\right) = \log q_e - \frac{k_1 t}{2.303}$ | $q_{e,\,exp}$ (mg/g) | 27 | 45 | 56 |
| | | $q_{e,cal}$ (mg/g) | 12.6 | 21.7 | 25.9 |
| | | $k_1$ (min$^{-1}$) | 0.016 | $3.24 \times 10^{-3}$ | $6.91 \times 10^{-3}$ |
| | | $R^2$ | 0.863 | 0.843 | 0.931 |
| Pseudo-second-order | $t/q_t = 1/k_2 q_e^2 + 1/q_e t$ | $q_{e,\,cal}$ (mg/g) | 25.6 | 43 | 52.6 |
| | | $k_2$ (g/mg.min) | $3.24 \times 10^{-3}$ | $1.71 \times 10^{-3}$ | $2.78 \times 10^{-3}$ |
| | | $R^2$ | 0.995 | 0.987 | 0.999 |
| Intraparticle diffusion | $q_t = k_d t^{0.5} + C$ | $k_d$ (mg/g min$^{1/2}$) | 1.31 | 2.05 | 1.74 |
| | | $C$ | 9.16 | 12.9 | 29.1 |
| | | $R^2$ | 0.707 | 0.892 | 0.881 |

from slope and intercept of linear plot of qt against $t^{0.5}$ as plotted in Fig. 8C.

The third model, an intraparticle diffusion model can describe numerous mechanisms through the adsorption process classified into three steps: (i) External surface adsorption, (ii) Intraparticle diffusion which was the rate-limiting step and (iii) The final equilibrium step which was very fast (Morris and Weber 1963). As shown in Fig. 8c, the plots of intraparticle diffusion model showed two stages of adsorption, which are not a straight line passing through origin. The first stage shows fast adsorption by surface adsorption and then followed by slow rate of intraparticle diffusion process (Yan et al. 2015; Fathy 2020; El-Shafey et al. 2021). Therefore, this model is not only the controlling-rate step

in adsorption of RY160 dye molecules onto the obtained carbon materials.

## Evaluation of adsorption isotherms

Langmuir, Freundlich, and Temkin adsorption isotherms (Langmuir 1918; Freundlich 1906; Temkin and Pyzhev 1940) were used to analyze equilibrium adsorption of RY160 dye onto carbon samples. Calculated parameters of these models are listed in Table 4. It can be observed that the correlation coefficients ($R^2$) of the applied kinetic models are approximately similar ($R^2$ varied from 0.95 to 0.98). This may confirm that active surface sites changes from homogeneous to heterogeneous character of adsorbent surface,

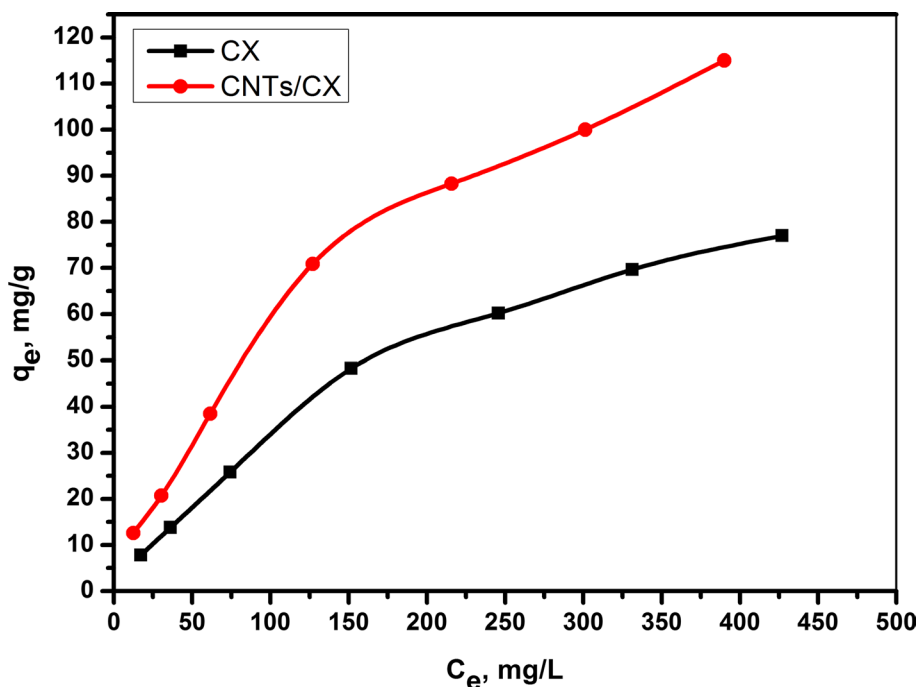**Fig. 9** Adsorption isotherms of RY160 dye on the prepared samples (pH = 4 and $T$ = 25 °C)

**Table 4** Adsorption isotherms, linear equations and the calculated parameters for the adsorption of reactive yellow dye on samples (pH = 4 and $T$ = 25 °C)

| Isotherms | Equation | Parameter | CX | CNTs/CX |
|---|---|---|---|---|
| Langmuir | $\frac{C_e}{q_e} = \frac{1}{K_L q_L} + \frac{1}{q_L} C_e$ | $q_L$ (mg/g) | 125 | 167 |
| | | $K_L$ (L/g) | $3.71 \times 10^{-3}$ | $3.51 \times 10^{-3}$ |
| | | $R_L$ | 0.350 | 0.363 |
| | | $R^2$ | 0.977 | 0.953 |
| Freundlich | $\ln q_e = \ln K_F + 1/n \ln C_e$ | $K_F$ (mg/g (l/mg)$^{1/n}$) | 1.11 | 2.24 |
| | | $1/n$ | 0.713 | 0.672 |
| | | $R^2$ | 0.964 | 0.987 |
| Temkin | $q_e = B \ln K_T + B \ln C_e$ | $B$ (kJ/mol) | 49.24 | 70.1 |
| | | $K_T$ (L/g) | 0.068 | 0.081 |
| | | $R^2$ | 0.965 | 0.955 |

**Table 5** A comparison between different adsorbents used for removal of the reactive yellow 160 dye

| Adsorbents | pH | Adsorption capacity ($q_L$, mg/g) | Refs. |
|---|---|---|---|
| Modified glauconite | 1 | 55.87 | Younes et al. (2021) |
| Alumina nanoparticles | 5 | 85.47 | Abdel Ghafar (2020a) |
| Nano sized magnetite mesoporous carbon | 3 | 62.80 | Toutounchi et al. (2019) |
| Zwitterionic Surfactant-modified Clay | 2 | 54.61 | Abdel Ghafar (2020b) |
| Micellar anionic surfactant | 12 | 4.76 | Sultana et al. (2021) |
| Carbon xerogel (CX) | 4 | 125 | This study |
| CNTs/CX | 4 | 167 | This study |

where the $R^2$ value of Freundlich model for adsorption RY160 dye onto CNTs/CX sample is the highest between $R^2$ values of other models. Thus the surface of CNTs/CX is more heterogeneity than CX.

Equilibrium adsorption data were plotted in Fig. 9 to show the type of adsorption, indicating that *F*-type (Freundlich) of adsorption can be fitted the adsorption of RY160 dye on both samples. From Langmuir model, the maximum adsorption capacity of CX and CNTs/CX toward RY160 dye removal was counted to be 125 and 167 mg/g, respectively; at pH = 4 and 25 °C. The adsorption of RY160 is a favorable process as indicated by the value of $R_L$ less than 1. The smaller $1/n$ value and higher $K_F$ value as calculated from Freundlich model for adsorption of RY160 dye on CNTs/CX sample confirmed that the adsorption of RY160 dye is more agreeable and greater intensity of the adsorption on CNTs/CX adsorbent than that occurred by CX. Moreover, value of B, Temkin constant, calculated from adsorption of RY160 dye on CNTs/CX is very higher than that adsorption by CX adsorbent; indicating the increase in adsorption capacity by obtained carbon hybrid (CNTs/CX) (Fathy et al., 2021a, b; Younes et al. 2021). From these results of adsorption isotherms, it can be concluded that the more heterogeneity surface is the more adsorption of reactive dyes on the surface of carbon from aqueous solutions. Overall, these findings approved that the obtained samples exhibited superior adsorption capacity toward RY160 dye comparing with other adsorbents in literature as shown in Table 5, which makes they are promising and feasible adsorbents for reactive dyes. Arguably, the synthesized carbon xerogels and its hybrid exhibited admirable adsorption capacity with comparing to

those of other adsorbents in the literature. Conclusively, the carbon-based hybrid represents a logical alternative for the treatment of the industrial wastewater charged with anionic reactive dyes.

# Conclusion

Here, the current study indicated that an incorporation of Fe–Ni catalysts onto RF organic xerogel by co-precipitation yielded good CX as substrate for growing CNTs through cracking camphor as evident by TEM and XRD tools. Equilibrium adsorption studies of anionic YR160 dye onto CX and CNTs/CX nanohybrid is depended highly on pH, initial dye concentrations, contact time and temperature. Adsorption process is spontaneous and exothermic in nature and attained equilibrium within 60 min with high adsorption rate at the beginning of removal process. Interestingly, the presence of CNTs changed the surface character of CX from homogenous to heterogeneous and boosted the adsorption capacity from 125 to 167 mg/g; increased by about ~ 34% with constant carbon dose 1 g/L at pH 4 and 25 °C. An intraparticle diffusion model affirmed that both surface adsorption and interparticle diffusion are the controlling-rate steps in the adsorption mechanism of RY160 dye. Therefore, this study reveals that CNTs/CX nanohybrid possesses considerable adsorption efficiency as compared with CX alone and others reported in the literature toward removal RY160 from their aqueous solutions. Therefore, this work opens a new avenue for obtaining adsorbents of CNTs/CX with highly active surface under the hereby described method.

## Declarations

## References

Abdel Ghafar HH, Radwan EK, Khalil NM, Algamal Y (2020a) Removal of reactive yellow 160 from aqueous solution by alumina nanoparticles derived from aluminum waste residue. Egypt J Chem 63:2887–2899

Abdel Ghafar HH, Radwan EK, El-Wakeel ST (2020b) Removal of hazardous contaminants from water by natural and zwitterionic surfactant-modified clay. ACS Omega 5:6834–6845

Annamalai KP, Fathy NA, Tao Y (2017) Synthesis and capacitance performance of phosphorous-enriched carbon xerogel. J Sol-Gel Sci Technol 48:515–521

Arenillas A, Menéndez JA, Reichenauer G, Celzard A, Fierro V et al (2019) Organic and Carbon Gels: From Laboratory to Industry? Organic and Carbon Gels: From Laboratory Synthesis to Applications. Springer, Cham, pp 1–26

Atieh MA, Bakather OY, Al-Tawbini B, Bukhari AA, Abuilaiwi FA, Fettouhi MB (2010) Effect of carboxylic functional group functionalized on carbon nanotubes surface on the removal of lead from water. Bioinorg Chem Appl 11:603978. https://doi.org/10.1155/2010/603978

Barka N, Abdennouri M, Makhfouk MEL (2011) Removal of methylene blue and eriochrome Black T from aqueous solutions by biosorption on Scolymus hispanicus L.: kinetics, equilibrium and thermodynamics. J Taiwan Inst Chem Eng 42:320–326

Bedolla-Guzman A, Sirés I, Thiam A, Peralta-Hernández JM, Gutiérrez-Granados S, Brillas E (2016) Application of anodic oxidation, electro-fenton and UVA photoelectro-fenton to decolorize and mineralize acidic solutions of Reactive Yellow 160 azo dye. Electrochim Acta 206:307–316

Celzard A, Fierro V, Amaral-Labat G (2012) Adsorption by carbon gels. In: Juan M. D. Tascón (ed) Novel carbon adsorbents. Elsevier (Copyright ©2012)

Chinnappan A, Baskar C, Kim H, Ramakrishna S (2016) Carbon nanotube hybrid nanostructures: future generation conducting materials. J Mater Chem A 4:9347

De Volder MFL, Tawfick SH, Baughman RH, Hart AJ (2013) Carbon nanotubes: present and future commercial applications. Science 339:535–539

El-Kholy SM, Fathy NA, Farag HK, Aboelenin MRM (2020) $In_2O_3$ catalyst supported on carbonaceous nanohybrid for enhancing the removal of methyl orange dye from aqueous solutions. Des Water Treat 174:344–353

El-Shafey OI, El-Shafey S, Fathy NA (2021) Mesoporous carbon xerogels adsorbents for adsorption of cadmium and p-nitrophenol pollutants: kinetic and equilibrium studies. Egypt J Chem 65(2):487–497

Embaby MA, Abdel Moniem SM, Fathy NA, El-kady AA (2021) Nanocarbon hybrid for simultaneous removal of arsenic, iron and manganese ions from aqueous solutions. Heliyon 7(10):e08218

Fang W, Liu L, Li R, Zhang R, Wang W, Zhang D, Cui Z (2020) Preparation of bimetal-based FeNi-N/C catalyst and its electrocatalytic oxygen reduction performance. SN Appl Sci 2:837. https://doi.org/10.1007/s42452-020-2651-1

Fathy NA (2020) Carbon-based nanomaterials for wastewater treatment, In: Abd-Elsalam Kamel (ed) Aqua nanotechnology: Applications of Nanomaterials for Water Purification. Elsevier (Copyright © 2020)

Fathy NA, Annamala PK, Tao Y (2017a) Effects of phosphoric acid activation on the nanopore structures of carbon xerogel/carbon nanotubes hybrids and their capacitance storage. Adsorption 23:355–360

Fathy NA, Lotfy VF, Basta AH (2017b) Comparative study on the performance of carbon nanotubes prepared from agro- and xerogels as carbon supports. J Analy Appl Pyrolysis 128:114–120

Fathy NA, Basta AH, Lotfy FV (2019a) Novel trends for synthesis of carbon nanostructures from Agricultural wastes. In: Abd-Elsalam Kamel (ed) Carbon Nanomaterials for Agri-food and Environmental Applications. Elsevier (Copyright ©2019a)

Fathy NA, El-Kholy SM, Aboelenin MRM (2019b) Carbon xerogel/carbon nanotubes nanohybrid doped with Ti for removal of methylene blue dye. Egypt J Chem 62:2277–2288

Fathy NA, El-Kholy SM, Ahmed SAS, El-Nabarawy TA, Tao Y (2021a) Superior adsorption of cationic dye on novel bentonite/carbon composites. Asia-Pac J Chem Eng. https://doi.org/10.1002/apj.2586

Fathy NA, El-Kholy SM, El-Shafey OI (2021b) Modified carbon nanostructures obtained from sugarcane bagasse hydrochar for treating chromium-polluted water. Current Analytical Chem 17:975–988

Freundlich HMF (1906) Over the adsorption in solution. J Phys Chem 57:385–470

Girgis BS, Attia AA, Fathy NA (2011) Potential of nano-carbon xerogels in the remediation of dye-contaminated water discharges. Desalination 265:169–176

Haghgoo M, Yousefi AA, Mehr MJZ, Celzard A, Fierro V, Léonard A, Job N (2014) Characterization of multi-walled carbon nanotube dispersion in resorcinol–formaldehyde aerogels. Micropor Mesopor Mater 184:97–104

Haghgoo M, Yousefi AA, Mehr MJZ, Léonard AF, Philippe MP, Compére P, Léonard A, Job N (2015) Correlation between morphology and electrical conductivity of dried and carbonized multi-walled carbon nanotube/resorcinol–formaldehyde xerogel composites. J Mater Sci 50:6007–6020

Halama A, Szubzda B, Pasciak G (2010) Carbon aerogels as electrode materials for electrical double layer supercapacitors – synthesis and properties. Electrochim Acta 55:7501–7505

Ho YS, McKay G (1998) Sorption of dye from aqueous solution by peat. Chem Eng J 70:115–124

Huang JQ, Zhang Q, Zhao MQ, Wei F (2012) A review of the large-scale production of carbon nanotubes: the practice of nanoscale process engineering. Chin Sci Bull 57:157–166

Iijima S (1991) Helical microtubules of graphite carbon. Nature 354:56–58

Indhu S, Muthukumaran K (2018) Removal and recovery of reactive yellow 84 dye from wastewater and regeneration of functionalised Borassus flabellifer activated carbon. J Environ Chem Eng 6:3111–3121

Job N, Théry A, Pirard R, Marien J, Kocon L, Rouzaud JN (2005) Carbon aerogels, cryogels and xerogels: influence of the drying method on the textural properties of porous carbon materials. Carbon 43:2481–2494

Kicínski W, Dyjak S, Tokarz W (2021) Carbon gel-derived Fe–N–C electrocatalysts for hydrogen-air polymer electrolyte fuel cells. J Power Sour 513:230537

Kiran Sh, Rafique MA, Iqbal S, Nosheen S, Naz S, Abdur Rasheed A (2020) Synthesis of nickel nanoparticles using *Citrullus colocynthis* stem extract for remediation of Reactive Yellow 160 dye. Environ Sci Poll Res 27:32998–33007

Kousha M, Tavakoli S, Daneshvar E, Vazirzadeh A, Bhatnagar A (2015) Central composite design optimization of acid blue 25 dye biosorption using shrimp shell biomass. J Mol Liq 207:266–273

Lagergren S (1898) Zurtheorie der sogenannten adsorption gelosterstoffe. Kungliga Svenska Vetenska Psakademiens Handlingar 24:1–39

Langmuir I (1918) The adsorption of gases on plane surfaces of glass, mica and platinum. J Am Chem Soc 40:1361–1403

Laurila T, Sainio S, Caro AM (2017) Hybrid carbon based nanomaterials for electrochemical detection of biomolecules. Prog Mater Sci 88:499–594

Li H, Song SI, Song GY, Kim I (2014) Non-covalently functionalized carbon nanostructures for synthesizing carbon-based hybrid nanomaterials. J Nanosci Nanotechnol 14:1425–1440

Morris J, Weber WJ (1963) Kinetics of adsorption on carbon from solution. J Saint Eng Div Am Soc Civil Eng 89:31–39

Mukul K, Xinluo Z, Yoshinori A, Sumio I, Maheshwar S, Kaori H (2002) Carbon nanotubes from camphor by catalytic CVD. Mol Cryst Liq Cryst 387:117–121

Navrotskaya AG, Aleksandrova DD, Krivoshapkina EF, Sillanpää M (2020) Hybrid materials based on carbon nanotubes and nanofibers for environmental applications. Front Chem 8:546

Prasek J, Drbohlavova J, Chomoucka J, Hubalek J, Jasek O, Adam V, Kizek R (2011) Methods for carbon nanotubes synthesis—review. J Mater Chem 21:15872–15884

Rashwan WE, Fathy NA, Elkhouly SM (2018) A novel catalyst of ceria-nanorods loaded on carbon xerogel for catalytic wet oxidation of methyl green dye. J Taiwan Inst Chem Eng 88:234–242

Shariati F, Shariati Sh, Moghaddam MAA (2021) Application of magnetite nanoparticles modified Azolla as an adsorbent for removal of reactive yellow dye from aqueous solutions. Desalin Water Treat 212:323–332

Shouman MA, Fathy NA (2018) Microporous nanohybrids of carbon xerogels and multi-walled carbon nanotubes for removal of rhodamine B dye. J Water Proc Eng 23:165–173

Sultana H, Usman M, ul Haq A, Mansha A (2021) Micellar enhanced flocculation for the effective removal of reactive yellow 160 from synthetic textile effluent. Environ Technol Innov 24:101896

Temkin MI, Pyzhev V (1940) Kinetic of ammonia synthesis on promoted iron catalyst. Acta Phys Chem URSS 12:327–356

Toutounchi S, Shariati S, Mahanpoor K (2019) Synthesis of nano-sized magnetite mesoporous carbon for removal of Reactive Yellow dye from aqueous solutions. Appl Organomet Chem 33(9):e5046

Worsley MA, Pauzauskie PJ, Kucheyev SO, Zaug JM, Hamza AV, Satcher JH, Baumann TF (2009) Properties of single-walled carbon nanotube-based aerogels as a function of nanotube loading. Acta Mater 57:5131–5136

Yan L, Qin LL, Yu HQ, Li S, Shan RR, Du B (2015) Adsorption of acid dyes from aqueous solution by CTMAB modified bentonite: kinetic and isotherm modeling. J Mol Liq 211:1074–1081

Younes H, El-Etriby HKh, Mahanna H (2021) High removal efficiency of reactive yellow 160 dye from textile wastewater using natural and modified glauconite. Int J Environ Sci Technol. https://doi.org/10.1007/s13762-021-03528-3

Zhang Q, Huang J-Q, Zhao M-Q, Qian W-Z, Wei F (2011) Carbon nanotube mass production: principles and processes. Chemsuschem 4:864–889

Zubizarreta L, Arenillas A, Domínguez A, Menédez JA, Pis JJ (2008) Development of microporous carbon xerogels by controlling synthesis conditions. J Non-Cryst Solids 354:817–825